REPRODUCTION
RESEARCH

Computational flow cytometry reveals that cryopreservation induces spermptosis but subpopulations of spermatozoa may experience capacitation-like changes

C Ortega-Ferrusola[2], L Anel-López[2], P Martín-Muñoz[1], J M Ortíz-Rodríguez[1], M C Gil[1], M Alvarez[2], P de Paz[3], L J Ezquerra[1], A J Masot[1], E Redondo[1], L Anel[2] and F J Peña[1]

[1]*Laboratory of Equine Reproduction and Equine Spermatology, Veterinary Teaching Hospital, University of Extremadura, Cáceres, Spain,* [2]*Reproduction and Obstetrics Department of Animal Medicine and Surgery, and* [3]*Department of Molecular Biology, University of León, León, Spain*

Correspondence should be addressed to F J Peña; Email: fjuanpvega@unex.es

Abstract

The reduced lifespan of cryopreserved spermatozoa in the mare reproductive tract has been attributed to both capacitative and apoptotic changes. However, there is a lack of studies investigating both phenomena simultaneously. In order to improve our knowledge in this particular point, we studied in raw and frozen-thawed samples apoptotic and capacitative markers using a wide battery of test based in flow cytometry. Apoptotic markers evaluated were caspase 3 activity, externalization of phosphatidylserine (PS), and mitochondrial membrane potential. Markers of changes resembling capacitation were membrane fluidity, tyrosine phosphorylation, and intracellular sodium. Conventional and computational flow cytometry using nonlinear dimensionally reduction techniques (*t*-distributed stochastic neighbor embedding (t-SNE)) and automatic classification of cellular expression by nonlinear stochastic embedding (ACCENSE) were used. Most of the changes induced by cryopreservation were apoptotic, with increase in caspase 3 activation ($P < 0.01$), PS translocation to the outer membrane ($P < 0.001$), loss of mitochondrial membrane potential ($P < 0.05$), and increase in intracellular Na+ ($P < 0.01$). Average values of markers of capacitative changes were not affected by cryopreservation; however, the analysis of the phenotype of individual spermatozoa using computational flow cytometry revealed the presence of subpopulations of spermatozoa experiencing capacitative changes. For the first time advanced computational techniques were applied to the analysis of spermatozoa, and these techniques were able to disclose relevant information of the ejaculate that remained hidden using conventional flow cytometry.

Reproduction (2017) **153** 293–304

Introduction

In spite of equine male gametes trade constituting a major component of the equine industry, cryopreservation of stallion spermatozoa, as an indispensable tool for the commerce of frozen-thawed semen doses, still has numerous drawbacks (Pena *et al.* 2011). To obtain acceptable fertility, intensive management of the mares is required to perform AI close enough to ovulation as the surviving spermatozoa have reduced lifespan in the mare's reproductive tract. This intensive management increases the costs related to insemination precluding a wider use of frozen-thawed semen. The reduced lifespan of the thawed sperm has been attributed to either changes similar to capacitation (Cormier *et al.* 1997, Pons-Rejraji *et al.* 2009) or changes that resemble apoptosis (Ortega-Ferrusola *et al.* 2008), or spermptosis as it has been recently termed (Gallardo Bolanos *et al.* 2014, Pena *et al.* 2016*b*). Capacitation is characterized by changes in sperm membrane fluidity, overall increase in tyrosine phosphorylation, and decrease in intracellular sodium (Escoffier *et al.* 2012), while spermptosis implies caspase activation, loss of mitochondrial membrane potential, and transposition of phosphatidylserine (PS) to the outer leaflet of the membrane (Ortega-Ferrusola *et al.* 2008, Ortega Ferrusola *et al.* 2009, Gallardo Bolanos *et al.* 2014). However, there is a lack of detailed studies analyzing both types of changes simultaneously. We aimed to focus our study on the surviving population of spermatozoa, to identify how characteristics related to apoptosis or capacitation change during this process in the same ejaculates following a split sample design. Recent developments in flow cytometry applied to sperm analysis are increasing the number of parameters that can be assessed simultaneously in a single assay (Gallardo Bolanos *et al.* 2014, Pena *et al.* 2015, Pena 2016*a*), this therefore demands the

ISSN 1470–1626 (paper) 1741–7899 (online)
DOI: 10.1530/REP-16-0539
Online version via www.reproduction-online.org

interpretation of the results due to the multidimensional nature of the data gathered, compared with the traditional bi-dimensional dot plots or uni-dimensional histograms. Moreover, the heterogeneous nature of the ejaculate is not disclosed in classical flow cytometry analysis based in manual gating. By using t-SNE data generated by multicolor flow cytometry can be represented in a two-dimensional (2D) plot, similar to biaxial plots, in which differences account for all the markers (Grimes *et al.* 2013). ACCENSE (Automatic Classification of Cellular Expression by Nonlinear Stochastic Embedding) is a tool that computes a 2D nonlinear distillation of the raw data, and automatically stratifies cells into phenotypic subpopulations based on their distribution of markers (Shekhar *et al.* 2014), avoiding the pitfalls derived from manual gating and classification of cells.

In view of these facts, we studied, in the same ejaculates following a split sample design, changes occurring after cryopreservation potentially related to capacitation (such as increase in tyrosine phosphorylation, increase in membrane fluidity, production of reactive oxygen species (ROS), and changes in intracellular Na+) and potentially related to apoptosis (such as mitochondrial membrane potential, activation of caspase 3, and transposition of PS). Moreover, we applied traditional and computational flow cytometry analysis to shed light on the changes that cryopreservation induces in the surviving spermatozoa population, and to disclose changes in the sperm subpopulation structure at the single cell level. We hypothesize that computational flow cytometry may improve our understanding of the changes induced by cryopreservation at the single cell level, disclosing changes in the sperm subpopulation structure of the ejaculates.

Materials and methods

Reagents and media

Merocyanine 540 (Excitation: 488 nm; Emission: 560 nm) (Ref: M24571); YO-PRO-1 (Excitation: 491 nm; Emission: 509 nm) (Ref: Y3603); Hoechst 33342 (Excitation: 350 nm; Emission: 461 nm) (Ref: H3570); 5,5′,6,6′-tetrachloro-1,1′,3,3′ tetraethyl benzimidazolyl carbocyanine iodine (JC-1) (Excitation: 488 nm; Emission: 530 nm, monomer form) (Excitation: 561 nm; Emission: 591 nm, aggregate form) (Ref: T3168); Annexin V Pacific Blue™ conjugate (Excitation: 410 nm, Emission: 455 nm) (Ref: A35122); CellROX Deep Red Reagent (Excitation: 644 nm; Emission: 655 nm) (Ref: C10422); Cell Event Caspase-3/7 Green Detection Reagent (Excitation: 502 nm; Emission: 530 nm) (Ref: C10423); ethidium homodimer (Excitation: 528 nm; Emission: 617 nm) (Ref: E1169); LIVE/DEAD® Fixable Violet Dead Cell Stain Kit (Excitation: 405 nm, Emission: 451 nm) (Ref: L34955) and Sodium Green cell permeant Indicator (Ref S-6901) (Excitation: 488 nm; Emission: 532 nm) were purchased from ThermoFisher Scientific (Molecular Probes). Phospho-Tyrosine Mouse mAb (P-Tyr-100) (PE conjugate) (Ref: 14967) was acquired from Cell Signalling Technology.

Semen collection and processing

Three ejaculates per horse were collected from 7 fertile stallions, which were maintained according to institutional and European regulations (Law 6/2013 June 11th and European Directive 2010/63/EU). The samples were obtained on a regular basis (three collections/week) during the 2016 breeding season. The ejaculates were obtained using a pre-warmed (45°C), lubricated Missouri model artificial vagina with an inline filter to eliminate the gel fraction. The semen was immediately transported to the laboratory for evaluation and processing. The ejaculates were separated in two aliquots, diluted 1:2 in INRA96 (IMV, L'Aigle, France), and centrifuged at 600 ***g*** for 10 min at room temperature. One of the aliquots was further extended in INRA 96 after centrifugation to obtain a final concentration of 100×10^6 spermatozoa/mL and was kept at room temperature (22°C) during 1 h for analysis as raw sperm controls. The other aliquot was diluted in the freezing medium Cáceres (University of Extremadura, Cáceres, Spain) containing 2% egg yolk, 1% glycerol, and 4% dimethylformamide to 100×10^6 spermatozoa/mL. After loading the extended semen into 0.5-mL straws (IMV, L'Aigle, France), the straws were ultrasonically sealed with UltraSeal 21® (Minitube of America MOFA, Verona, WI, USA) and immediately placed in an IceCube 14S (SY-LAB, Neupurkersdorf, Austria) programmable freezer. The following freezing curve was used. Straws were kept for 15 min at 20°C, and they were then slowly cooled from 20°C to 5°C at a cooling rate of 0.1°C/min. Thereafter the freezing rate was increased to –40°C/min from 5°C to –140°C. The straws were then plunged into liquid nitrogen and stored until analysis. For the analysis, two straws per stallion and freezing operation were thawed in a water bath at 37°C for at least 30 s and diluted in pre-warmed INRA 96 extender to a final concentration of 50×10^6 spermatozoa/mL. All analyses were conducted immediately after thawing.

Flow cytometry

Flow cytometry analyses were conducted using two equipments: a MACSQuant Analyzer 10 (Miltenyi Biotech) flow cytometer equipped with three lasers emitting at 405, 488, and 635 nm and 10 photomultiplier tubes (PMTs): V1 (excitation 405 nm, emission 450/50 nm), V2 (excitation 405 nm, emission 525/50 nm), B1 (excitation 488 nm, emission 525/50 nm), B2 (excitation 488 nm, emission 585/40 nm), B3 (excitation 488 nm, emission 655–730 nm (655LP + split 730)), B4 (excitation 488 nm, emission 750 LP), R1 (excitation 635 nm, emission 655–730 nm (655LP + split 730)), and R2 (excitation 635 nm, emission filter 750 LP); and a MACSQuant® VYB (Miltenyi Biotech) flow cytometer equipped with yellow, violet, and blue lasers (561, 405, 488 nm) with 10 optical channels for multiparameter flow cytometry. The system was controlled using MACS Quantify software. The quadrants or regions used to quantify the frequency of each sperm subpopulation depended on the particular assay. Forward and sideways light scatter was recorded for a total of 50,000 events

per sample. Gating the sperm population after Hoechst 33342 staining eliminated non-sperm events. The instruments were calibrated daily using specific calibration beads provided by the manufacturer, and a compensation overlap was performed before each experiment. The data were analyzed using FlowJo V 10.2 Software (Ashland, OR, USA). Unstained, single stained, isotype, and Fluorescence Minus One (FMO) controls were used to determine compensations and positive and negative events, as well as to set regions of interest as described in previous publications from our laboratory (Pena *et al.* 2003, Gallardo Bolanos *et al.* 2014) (data not shown).

Simultaneous flow cytometric assessment of caspases 3 and 7 activity, viability, and oxidative stress (ROS)

CellEvent Caspase-3/7 Green Detection Reagent is a fluorogenic substrate for activated caspases 3 and 7. The reagent consists of a four-amino-acid peptide (DEVD) conjugated to a nucleic acid-binding dye. This cell permeant substrate is intrinsically non-fluorescent because the DEVD peptide inhibits the ability of the dye to bind to DNA. After activation of caspase 3 and caspase 7 in apoptotic cells, the DEVD peptide is cleaved, enabling the dye to bind to DNA and produce a bright, fluorogenic response with an absorption/emission maxima of 502/530 nm. Spermatozoa exhibiting oxidative stress emit fluorescence in the far-red spectrum, whereas Hoechst 33342-positive sperm emit blue fluorescence. The semen samples were diluted in PBS for staining to a final concentration 5×10^6 spermatozoa/mL. Then, cells were stained with 1 µL of CellROX (5 µM), 1 µL CellEvent Caspase-3/7 Green Detection Reagent (2 mM), and 0.3 µL of Hoechst 33342 (0.5 µM). After thorough mixing, the sperm suspension was incubated at room temperature in the dark for 25 min, washed in PBS, and loaded with 0.3 µL ethidium homodimer (1.167 mM in DMSO) to each sample. After incubation for a further 5 min, the samples were immediately run on the flow cytometer. The controls consisted of unstained and single stained controls to properly set gates and compensations. The positive controls for oxidation and caspase activation were samples supplemented with 800 µM SO_4Fe_2 and 1.7 M H_2O_2 (Sigma) to induce the Fenton reaction (Gallardo Bolanos *et al.* 2014). The debris were gated out based on the DNA content of the events after Hoechst 33342 staining.

Simultaneous assessment of mitochondrial activity and PS translocation

The mitochondrial potential was assessed by 5,5′,6,6′-tetrachloro-1,1′,3,3′ tetraethyl benzimidazolyl carbocyanine iodine (JC-1). This probe forms multimeric aggregates in mitochondria with high membrane potential (active mitochondria) and these aggregates emit in the high orange wavelength of 595 nm when excited at 561 nm (yellow laser). In mitochondria with low membrane potential (inactive mitochondria), JC-1 forms monomers that emit in the green wavelength (530 nm) when excited at 488 nm. Apoptosis-like changes were detected in spermatozoa with the use of Annexin V, Pacific Blue™ conjugate (Dead Cell Apoptosis Kit, Molecular Probes), which detects the translocation of PS from the inner to the outer leaflet of the plasma membrane associated with membrane changes related to sperm processing. Apoptotic cells show violet fluorescence (455 nm) when excited with the violet laser (405 nm). Both stains were combined in a multiparametric test and evaluated by FC. A final concentration of 5×10^6 spermatozoa/mL was obtained by adding 10 µL of diluted spermatozoa to 990 µL of PBS. The samples were loaded with 0.5 µL JC-1 (0.3 µM) and incubated at 37°C for 40 min. The samples were washed in PBS by a short centrifugation spin for 12′ and suspended in 100 µL of Annexin binding buffer (10 mM HEPES, 140 mM NaCl, 2.5 mM $CaCl_2$, pH 7.4). To 100 µL of sample per assay, 5 µL of Annexin V, Pacific Blue™ were added. After 15 min of incubation in the dark at room temperature, 400 µL of 1× Annexin binding buffer were added. Cytometry analysis was then performed using a MACSQuant® VYB (Miltenyi Biotech) flow cytometer with the yellow and violet lasers (561, 405 nm).

Evaluation of fluidity (lipid disorder) of the sperm membrane

Fluidity of sperm membranes was assessed with Merocyanine 540 (488–560 nm) (blue laser, channel B2) (Molecular Probes Europe) and membrane changes were detected with YO-PRO-1 (491–509) (blue laser, channel B1) (Molecular Probes Europe). Hoechst 33342 (350–461 nm) (violet laser, channel V1) was also incorporated to gate out debris. FC analyses were carried out with a MACSQuant Analyzer 10 (Miltenyi Biotech, Pozuelo de Alarcón, Madrid, Spain). A suspension of 5×10^6 spermatozoa was obtained by adding 10 µL of diluted spermatozoa to 990 µL of PBS. The samples were loaded with Merocyanine 540 at a final concentration of 2.7 µM, YO-PRO-1 25 nM, and 0.3 µM Hoechst 33342 and incubated in the dark for 30 min. The cells were washed in PBS by a short centrifugation spin for 12′, before reading in the FC. While Merocyanine 540 attaches to the sperm membrane and fluoresces in orange proportionally to the grade of membrane disorder present, YO-PRO-1 is a high-affinity nucleic acid stain that penetrates cells with compromised plasma membrane, fluorescing in green when is excited at 488 nm.

Assessment of tyrosine phosphorylation

The anti-phospho-Tyrosine Mouse mAb (P-Tyr-100) (PE conjugate) was used to detect the phosphorylation of tyrosine. The samples (1 mL) containing 10×10^6 spermatozoa/mL in PBS were stained with 1 µL of LIVE/DEAD violet Fixable Dead Cell Stain Kit Solution. After thorough mixing, the samples were incubated at room temperature (22°C) for 30 min in the dark. Then, the spermatozoa were washed with PBS (1×) and fixed with 900 µL of 4% paraformaldehyde and incubated for 10 min at 37°C. Afterwards, samples were incubated for 1 min on ice. The aliquots were washed by centrifugation twice. For the permeabilization, pre-chilled cells were slowly resuspended in ice cold 100% methanol to a final concentration of 90% methanol. The samples were incubated 30 min on ice. Then, the spermatozoa were washed in incubation buffer (0.5 g bovine serum albumin (BSA) in 100 mL 1× PBS) twice. The cells were loaded with 2 µL/mL Phosphor-Tyrosine Mouse mAb (P-Tyr-100) (PE conjugate) (50 µg/mL # 14967), and incubated for 30 min at room temperature (22°C) in the dark

after thorough mixing. Then, the spermatozoa were washed in 500 µL PBS. Finally, the samples were washed again in PBS before reading in the flow cytometer

Determination of intracellular Na+

The amount of intracellular Na+ in stallion spermatozoa was determined flow cytometrically after loading the cells with Sodium Green Permeant (5 µM), and incubated at r.t. 30′. Finally, samples were washed in PBS and dead spermatozoa were excluded from the analysis after ethidium homodimer staining (0.35µM 5′ at room temperature).

Computational flow cytometry (t-SNE analysis and ACCENSE)

Flow cytometry data are usually analyzed using a series of 2D plots and manual gating, however, the increase in the number of parameters measured increase the number of 2D plots to display for every marker combination. For example, a combination of four colors will require 30 2D plots. To overcome these problems computational methods to automatically identify populations in multidimensional flow cytometry data have been developed (Mair *et al.* 2016). Using FlowJo v 10.2 and ACCENSE software available at http://www.cellaccense.com, compensated data of each multiparametric assay described in the Materials and methods section were exported as FCS files from the flow cytometer, and loaded in FlowJo and ACCENSE for computational analysis. Data were concatenated and single cell events analyzed. Flow cytometry data were analyzed using nonlinear dimensionally reduction techniques (t-SNE) and ACCENSE. The Barnes–Hut implementation of t-SNE was used for low-dimensional embedding to perform dimensional reduction of cytometry data, classification of cells was based in *K* means techniques with the significance level set at $P=0.0001$, and data of all subpopulations generated were exported as FCS files. ACCENSE identifies clusters within multidimensional data without losing single cell resolution (Shekhar *et al.* 2014, Chester & Maecker 2015), allowing automatic gating of cells.

Statistical analysis

Three ejaculates were collected from each of the 7 individual stallions. All experiments were repeated at least three times with independent samples (three separate ejaculates from each of the seven stallions). The normality of the data was assessed using the Kolmogorov–Smirnov test. Since the data showed equivalence of variance, the results were analyzed by ANOVA followed by a Tukey *post hoc* test to perform pair-wise comparisons (SPSS 19.0 for Mac). Differences were considered significant when $P<0.05$, and are indicated as $*P<0.05$ and $**P<0.01$. Results are displayed as mean ± S.E.M.

Results

Changes induced by cryopreservation in caspase 3 activation, viability, and ROS production

Representative cytograms and gating strategies of the assay are given in Figure 1. The conventional flow cytometry analysis applied made evident that cryopreservation induced an increase in the percentage of spermatozoa expressing active caspases 3 and 7 (Fig. 2A). Paradoxically, ROS production was reduced in thawed samples (Fig. 2B and C). However, this reduction was not observed in a population of caspase 3-positive spermatozoa (Fig. 2B). The embedding (t-SNE) and clustering steps in ACCENSE revealed a complex structure of the ejaculate identifying more than 100 sperm subpopulations both in raw sperm and after freezing and thawing (Fig 3A, B, C, and D, E, F). Visualization of the structure of the ejaculate allowed identifying easily changes in the expression of caspase 3 as a result of the cryopreservation (Fig. 3B and E). The algorithm also gave FCS files of every subpopulation in the complex ejaculate structure: Figure 3G and H shows representative overlays of characteristic subpopulations in fresh sperm (in general, low caspase 3 expression and high superoxide production) and Figure 3I and J shows representative overlays in frozen and thawed samples characterized by low superoxide production and high caspase 3 activity. Reduction of multidimensional data to 2D plots using t-SNE in FlowJo to visualize changes in the sperm subpopulation structure of viable spermatozoa after cryopreservation (Fig. 4) revealed interesting changes; virtually all spermatozoa experienced changes after cryopreservation, with increases in the caspase activation, reduction of live spermatozoa, and changes in the position of sperm subpopulations in the 2D structure as the most relevant.

Changes in mitochondrial membrane potential (ΔΨm) and PS transposition to the outer leaflet of the membrane (Annexin assay) after cryopreservation

Cryopreservation induced a massive transposition of PS to the outer leaflet of the sperm membrane (Fig. 5I), and also reduced the membrane potential (Ψφm) of sperm mitochondria (Fig. 5J), with hierarchical gating showing that this effect occurred principally in Annexin + spermatozoa (Fig. 5G and H). When ACCENSE analysis was applied based in these markers, once again a complex subpopulation structure of the ejaculate was evident, with more than 100 distinct subpopulations revealed both in raw semen and after freezing and thawing (Fig. 5A, C, D, and F). Visualization of the t-SNE maps after ACCENSE gating and classification allowed identification of phenotypic changes in the presence of PS in the outer membrane (Fig. 6 A and D) and in the mitochondrial membrane potential (Fig. 6 B, E high Ψφm and C, F low Ψφm). Subpopulations in fresh sperm with PS transposition were evident in raw sperm (Fig. 5B) that were not obvious in the conventional analysis, expression of PS in the outer membrane increased after cryopreservation (Fig. 6D). ACCENSE analysis also revealed changes in mitochondria after cryopreservation with a general reduction in mitochondrial membrane

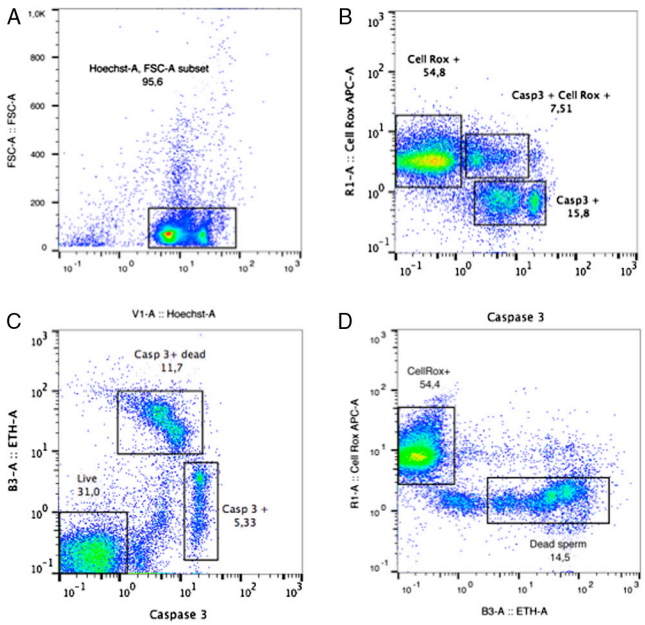

Figure 1 Representative cytograms of the simultaneous study of live and dead spermatozoa, caspase 3 and 7 activation, and production of reactive oxygen species. Samples were processed and stained as described in materials and methods. (A) Gating strategy to remove debris and cell clumps from the analysis, only H33342-positive (DNA-bearing) events were used in further analysis. Events not containing significant amounts of DNA (debris) or events containing DNA but with high area in FSC (doublets, clumps) were removed from the assay. (B) Dot plots reporting caspase 3 activity and reactive oxygen species production. (C) Dot plots reporting live spermatozoa, spermatozoa with caspase 3 activity, and dead spermatozoa. (D) Dot plots reporting production of reactive oxygen species and dead spermatozoa.

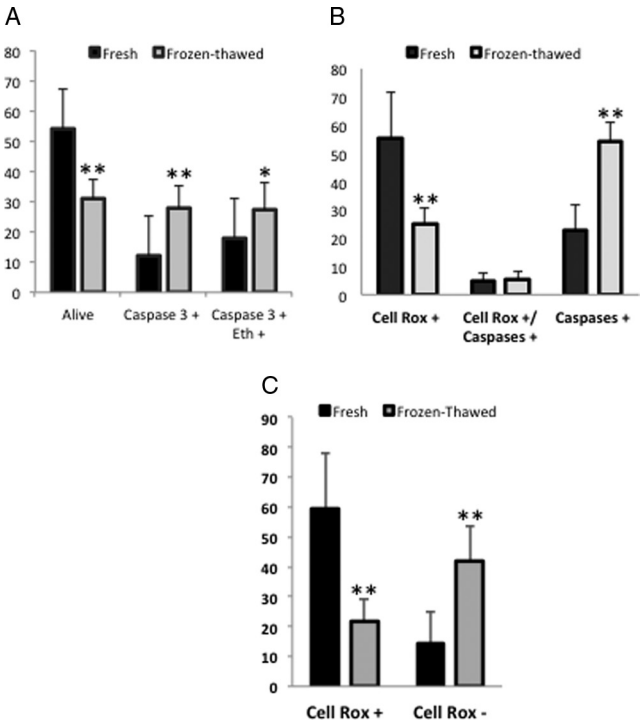

Figure 2 Changes in caspase 3 activation and production of reactive oxygen species after cryopreservation. Semen was processed and samples stained and analyzed as described in materials and methods. (A) Percentages of live, caspase+, and dead spermatozoa before and after cryopreservation. (B) Production of reactive oxygen species ROS (CellROX) before and after cryopreservation in caspase 3+ and caspase 3– spermatozoa. (C) Overall changes in ROS production as a consequence of cryopreservation $^{*}P<0.05$, $^{**}P<0.01$.

potential, although subpopulations of spermatozoa with high Ψφm remained (Fig. 6B and E). ACCENSE analysis provided FCS files of all the subpopulations originated; representative overlay cytograms of subpopulations in fresh and frozen-thawed samples are given in Figure 6G and H subpopulations in raw sperm were characterized by high Ψφm, and low PS externalization (H) while subpopulations in thawed samples show low Ψφm and PS externalization (I).

Evaluation of changes in membrane fluidity induced by cryopreservation

Cryopreservation reduced the fluidity of the sperm membranes (Fig. 7A, D, and E), however, also induced significant increases in Yo-Pro-1 uptake indicating increased membrane permeability and compromised membranes (Fig. 7B, C, D, and E).

The t-SNE analysis and visualization of the subpopulation structure revealed that cryopreservation induced dramatic changes in the structure of the ejaculate; downsampling and concatenation revealed that both raw sperm and frozen-thawed samples conserved two subpopulations of high and low merocyanine fluorescence (Fig. 8B and D). However, it was evident that in thawed samples the difference among these subpopulations was higher (Fig. 8D) than in raw sperm (Fig. 8B). The analysis of the phenotype of the spermatozoa using ACCENSE revealed that true subpopulations of high mero fluorescence were more common in fresh sperm than in thawed samples, where most of the spermatozoa showing high mero fluorescence also showed high Yo-Pro-1 uptake (Fig. 8A, B, D, and E). Overlay of sperm phenotypes in the t-SNE map revealed that the major change after freezing and thawing was an increase in Yo-Pro-1 uptake (green population in Figure 9C and F).

Changes in tyrosine phosphorylation induced by freezing and thawing

When conventional gating was applied, no major changes were observed in the intensity of the fluorescence of the phosphorylated proteins (Fig. 10C), the gating strategy to identify tyrosine phosphorylation

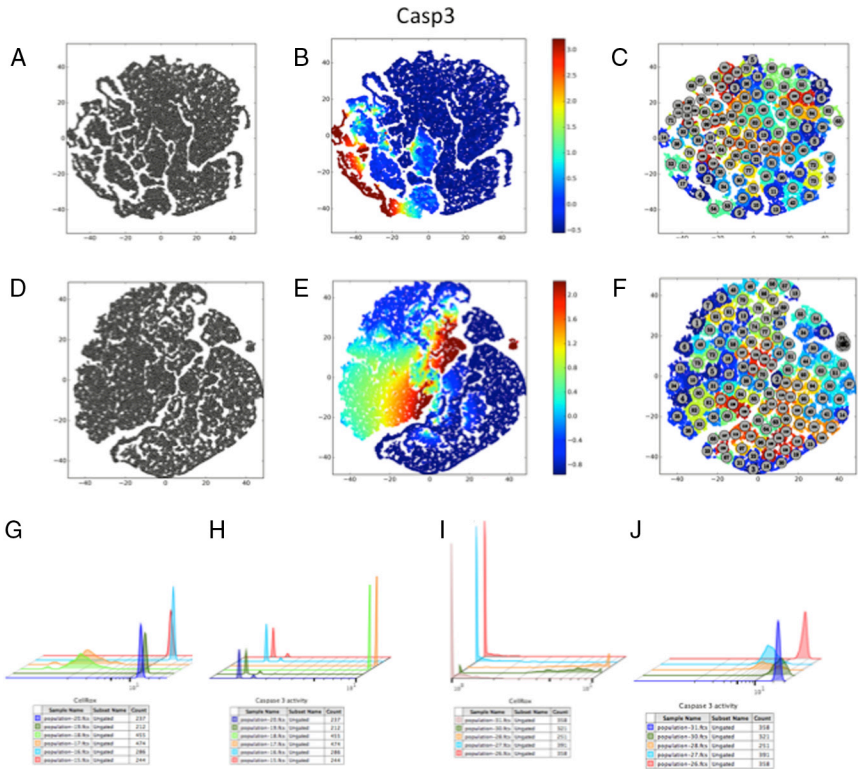

Figure 3 ACCENSE applied to high-dimensional multicolor cytometry data. (A and D) The 2D t-SNE maps of stallion spermatozoa after multicolor staining (H 33342, caspase 3 eth and CellROX) in fresh (A) and frozen-thawed spermatozoa (D). Each point represents a cell derived by downsampling from the original dataset. (B and E) Density map representing the intensity of caspase 3 activity in raw (B) and thawed (E) stallion spermatozoa, caspase activity increased after cryopreservation (see heat maps on the right). (C–F) Composite map depicting the complex structure of the stallion ejaculate; circles represent centers of phenotypically distinct subpopulations ($P=0.001$). (G–J) Representative overlays of phenotypic characteristics of events in different subpopulations in fresh (G–I) and frozen-thawed (H–J) spermatozoa.

is depicted in Figure 10D, E, F, and G. But when computational cytometry techniques were applied to the analysis, the t-SNE map and automatic ACCENSE classification of spermatozoa revealed that overall intensity of phosphorylation in tyrosine of sperm proteins was higher in fresh samples, and was reduced after cryopreservation, with the exception of a subpopulation of spermatozoa showing high intensity in both raw spermatozoa and thawed samples (Fig. 10A and B).

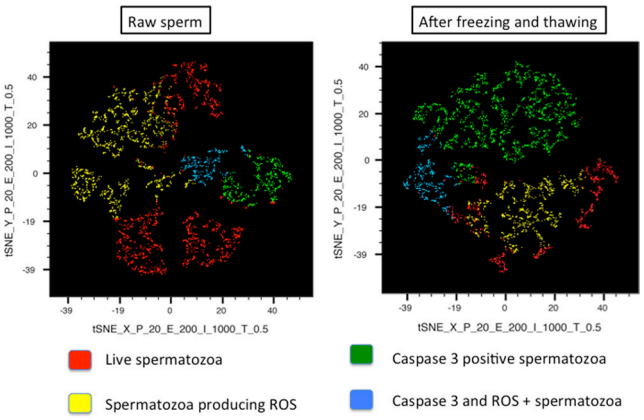

Figure 4 Examples of t-SNE maps generated in FlowJo V.10.2 showing overlays of distinct phenotypes of spermatozoa in raw and frozen-thawed stallion spermatozoa (only spermatozoa surviving cryopreservation). Red represents live spermatozoa; yellow represents live spermatozoa producing ROS, but not expressing caspase 3 activity; green represents spermatozoa showing caspase 3 activity, and blue represents spermatozoa producing ROS and expressing caspase 3 activity.

Changes in intracellular Na+ after cryopreservation

We used flow cytometry to investigate how intracellular Na+ changes during cryopreservation; the population of dead spermatozoa was gated out from the analysis after PI staining (Fig. 11B). Cryopreservation resulted in an increase in the content of intracellular Na+ in the spermatozoa surviving cryopreservation (Fig. 11A and C).

Discussion

In this study we evaluated and compared changes induced by cryopreservation that may relate to apoptosis (spermptosis) or to capacitation (cryocapacitation) in the same ejaculates following a split sample design. Moreover, for the first time we applied to sperm analysis techniques of computational flow cytometry allowing automatic gating and the identification of phenotypically distinct sperm subpopulations after flow cytometry analysis. The heterogeneous nature of the mammalian ejaculate has been recognized; different subpopulations of spermatozoa can be distinguished based on, for example, morphometric and kinetic analysis (Aparicio *et al.* 2005, Nunez-Martinez *et al.* 2006, 2007, Pena *et al.* 2006, Ortega-Ferrusola *et al.* 2009). This complex and heterogeneous nature has been

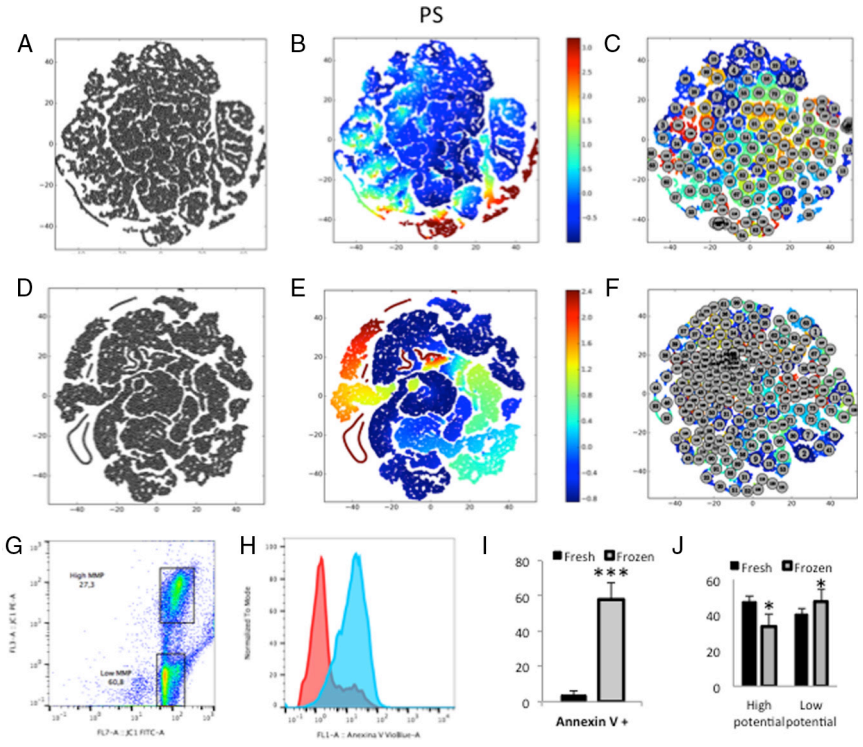

Figure 5 ACCENSE applied to high-dimensional multicolor cytometry data. (A and D) The 2D t-SNE maps of stallion spermatozoa after multicolor staining (Anexin-V and JC-1) in fresh (A) and frozen-thawed spermatozoa (D). Each point represents a cell derived from downsampling from the original dataset. (B and E) Density map representing the intensity of PS externalization in raw (B) and FT samples (E) of stallion spermatozoa, PS externalization increased after cryopreservation, although subpopulations with increased PS externalization were already evident in raw semen (see heat map bar at the right of each t-SNE map). (C–F) Composite map depicting the complex structure of the stallion ejaculate; circles represent centers of phenotypically distinct subpopulations ($P=0.001$). (G) Representative dot plots of the JC-1 assay (H) Representative overlay histograms of PS expression in raw semen (red) and thawed spermatozoa (blue). (I) Changes in the percentage of spermatozoa showing PS transposition and (J) changes in mitochondrial membrane potential induced by cryopreservation $^{*}P<0.05$, $^{***}P<0.001$.

identified in many different biological systems (Newman & Weissman 2006, Newman *et al.* 2006) and its importance also stressed in different aspects of medicine (Sigal *et al.* 2006, Cohen *et al.* 2008, Saadatpour *et al.* 2015). The heterogeneous nature of the spermatozoa has led to the consensus of the limited value of the report of average values in the sperm analysis (Newton 1998). Here, for the first time we have disclosed sperm subpopulations using computational flow cytometry approaches, and these techniques are powerful tools to identify sperm subpopulations in the ejaculate. Most dramatic changes in the spermatozoa surviving cryopreservation were related to apoptotic changes, with intense caspase 3 activation as the most evident change of all the parameters studied using both conventional and computational flow cytometry. This finding confirms

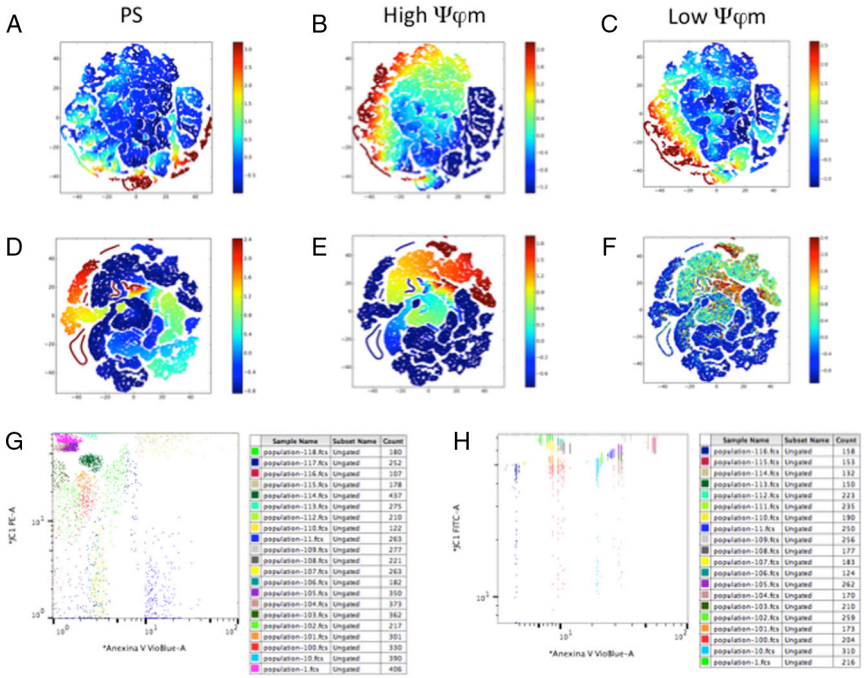

Figure 6 ACCENSE-derived t-SNE maps depicting channels for each phenotype marker in stallion spermatozoa in raw and thawed stallion spermatozoa. (A and D) Modifications in the externalization of PS after cryopreservation. (B–E) Changes in the mitochondria showing high Ψφm. (C–F) Changes in the mitochondria showing low Ψφm. (G and H) 20 representative subpopulations of spermatozoa in raw and frozen-thawed stallion spermatozoa, subpopulations in raw sperm were characterized by low PS and high Ψφm, while subpopulations in thawed spermatozoa were characterized by high PS externalization and low Ψφm.

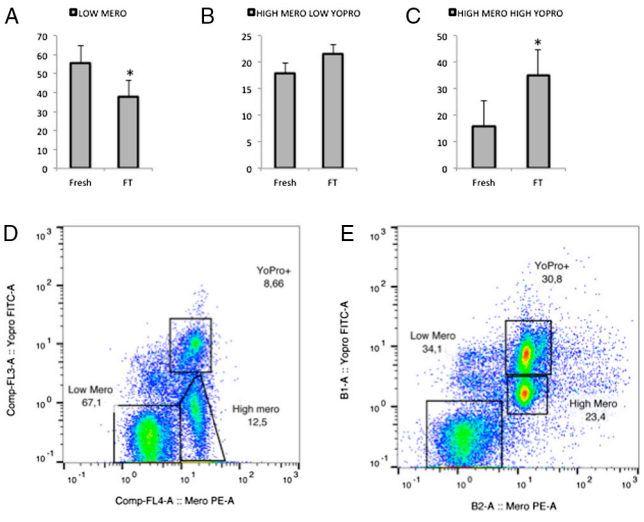

Figure 7 Evaluation of membrane fluidity. Stallion sperm was processed and stained as described in materials and methods. (A) Percentage of spermatozoa depicting low Merocyanine 540 fluorescence corresponding to membranes with low fluidity. (B) Percentage of spermatozoa with high membrane fluidity. (C) Percentage of spermatozoa with high Merocyanine 540 floruescence and high Yo-Pro1 uptake indicating compromised membranes. Comparisons are made between raw and n spermatozoa. $^{*}P < 0.05$. (D–E) Representative cytograms of the assay.

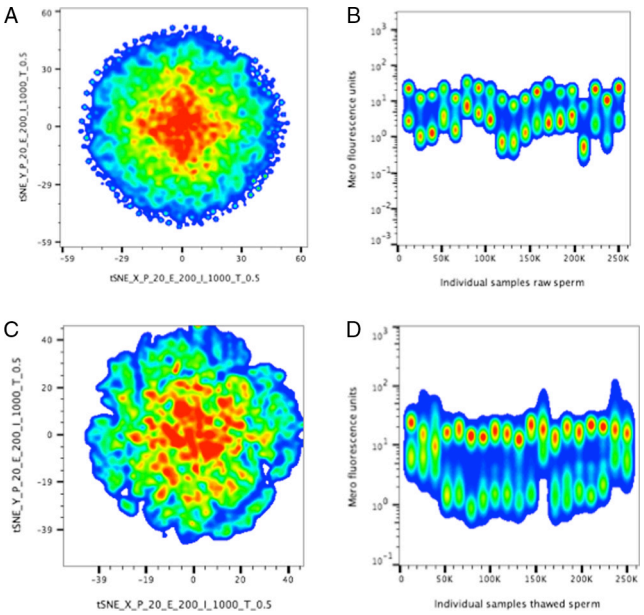

Figure 8 t-SNE maps of fresh and frozen-thawed spermatozoa after downsampling and concatenation using FlowJo v 10.2 plugins. Cryopreservation induced a major change in the sperm subpopulation structure (compare (A and C) t-SNE maps). In (B and D) concatenated samples in raw (B) and frozen-thawed (D) samples are compared. Two subpopulations are evident in all samples (high and low Merocyanine 540 fluorescence); however, in thawed samples the separation among populations with high and low Merocyanine 540 fluorescence is greater than in raw spermatozoa.

previous reports indicating that cryopreservation activates apoptotic phenomena (Pena *et al.* 2009, Ortega Ferrusola *et al.* 2010, Gallardo Bolanos *et al.* 2012, Caselles *et al.* 2014, Gallardo Bolanos *et al.* 2014, Kopeika *et al.* 2015, Pena *et al.* 2015, Munoz *et al.* 2016). Other features typical of apoptosis were also evident in our study including PS transposition and decreases in the mitochondrial membrane potential. An apparently paradoxical finding occurred, cryopreservation reduced ROS production; however, similar findings have been recently reported (Gibb *et al.* 2014, Yeste *et al.* 2015, Munoz *et al.* 2016). This is explained based in two factors: on one hand, the probe used in our study is specially sensitive to the superoxide anion ($O_2^{\bullet -}$) (Plaza Davila *et al.* 2015) and, on the other hand, mitochondria are the main source of ROS in the spermatozoa (Plaza Davila *et al.* 2015), so it is not surprising that reduced mitochondrial activity in thawed sperm (Pena *et al.* 2015) leads to decreased production of $O_2^{\bullet -}$. Markers of capacitation were also evaluated, including the fluidity of the sperm membranes and tyrosine phosphorylation of sperm proteins. Conventional flow cytometry revealed a reduction in the percentage of spermatozoa showing low membrane fluidity in cryopreserved samples; however, increases in membrane fluidity were also accompanied by increased Yo-Pro-1 uptake, suggesting early damage in the membrane instead of capacitation. The t-SNE analysis revealed not only a subpopulation of spermatozoa with increased membrane fluidity, but also increased Yo-Pro-1 uptake after thawing. Since an overall increase in tyrosine phosphorylation of sperm proteins is considered a hallmark of capacitation, this was investigated in fresh and thawed samples. There was not a significant increase in tyrosine phosphorylation after thawing. On the other hand, ACCENSE analysis revealed that increased tyrosine phosphorylation occurred only in a subpopulation of spermatozoa. Finally, since it has been shown that capacitation is associated with reduced intracellular Na+ (Escoffier *et al.* 2012), modifications in the sperm concentration of this ion were studied. We observed an increase in intracellular Na+ after cryopreservation; disruption of the Na+/K+ pump has been linked to cell shrinkage associated with apoptosis in many cell systems (Bortner & Cidlowski 2003, Iurinskaia *et al.* 2010, Sapia *et al.* 2010, Orlov *et al.* 2013, Honisch *et al.* 2014). In spermatozoa, reduced intracellular ATP associated with mitochondrial dysfunction (Plaza Davila *et al.* 2015, Davila *et al.* 2016) may explain increased intracellular Na+ in thawed samples.

Markers related with apoptosis were more evident in thawed samples; however, markers related to capacitation appeared only in specific subpopulations of thawed spermatozoa. Capacitation only occurs in a small percentage of cells (Bahat *et al.* 2003, Eisenbach 2003, Eisenbach & Giojalas 2006, Spiegel *et al.* 2006), this is in agreement with our findings. Capacitation is a

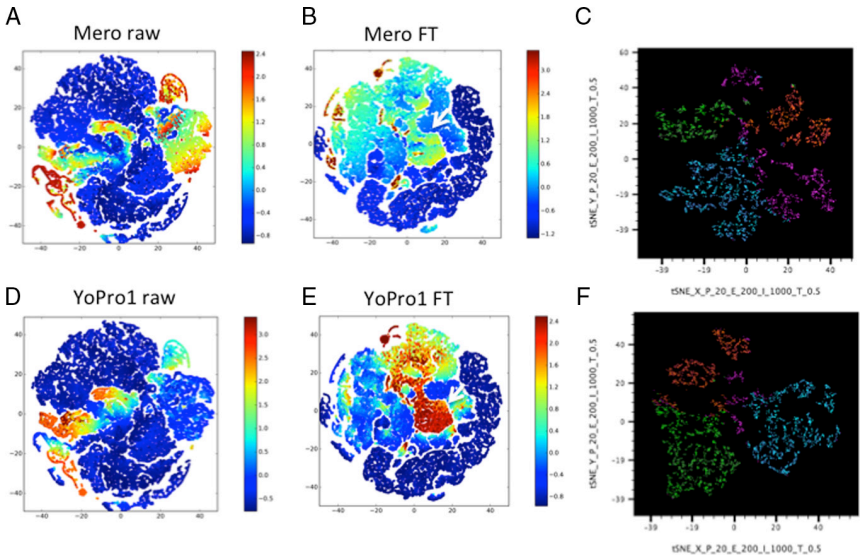

Figure 9 ACCENSE-derived t-SNE maps depicting channels for each phenotype marker in stallion spermatozoa in raw (A and D) and thawed (B and E) stallion spermatozoa. The intensity of Merocyanine 540 fluorescence and of the Yo-Pro1 uptake across the whole population of spermatozoa is depicted in a heat map. Comparing Merocyanine 540 fluorescence and Yo-Pro1 uptake allows to determine that in thawed samples the highest uptake of Yo-Pro1 corresponds also to high mero florescence (arrows). (C–F) t-SNE maps showing overlays of distinct sperm subpopulations in raw and frozen-thawed sperm, the most evident changes is an increase in the subpopulation of high Yo-Pro-1 uptake (in green) in thawed samples.

redox-regulated process, with increased ROS activating a soluble adenylyl cyclase that stimulates cAMP and PKA; the latter activates SRC kinases and suppresses an inhibitor of SRC. SRC phosphorylates and inactivates a protein phosphatase permitting a dramatic upregulation of tyrosine phosphorylation that characterizes capacitation (Salicioni *et al.* 2007, Buffone *et al.* 2014, Aitken *et al.* 2015, Alvau *et al.* 2016). Increased production of H_2O_2 leads to inhibition of tyrosine phosphatase activity, contributing also to increased tyrosine phosphorylation. Thus is not surprising that under conditions of reduced production of mitochondrial ROS, tyrosine phosphorylation is reduced, as seen in our experiments. It has been proposed that capacitation and apoptotic changes share a common

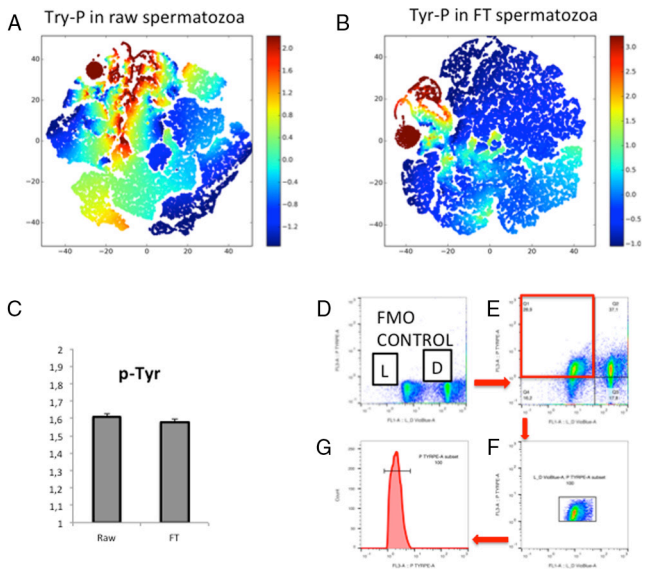

Figure 10 ACCENSE-derived t-SNE maps depicting channels for the intensity of tyrosine phosphorylation in the whole population of spermatozoa after downsampling and dimensional reduction. (A) Raw stallion spermatozoa. (B) Thawed stallion spermatozoa; although overall phosphotyrosine expression is reduced, a subpopulation with high expression appear in FT sperm. (C) Average fluorescence intensity in raw sperm and in frozen-thawed samples. (D–G) Gating strategy; D: fluorescence minus one (FMO) control and live a dead spermatozoa. (E–F) The region of live sperm phosphotyrosine-positive is gated to further analysis. (G) Histogram showing intensity of the fluorescence of phosphotyrosine-positive events.

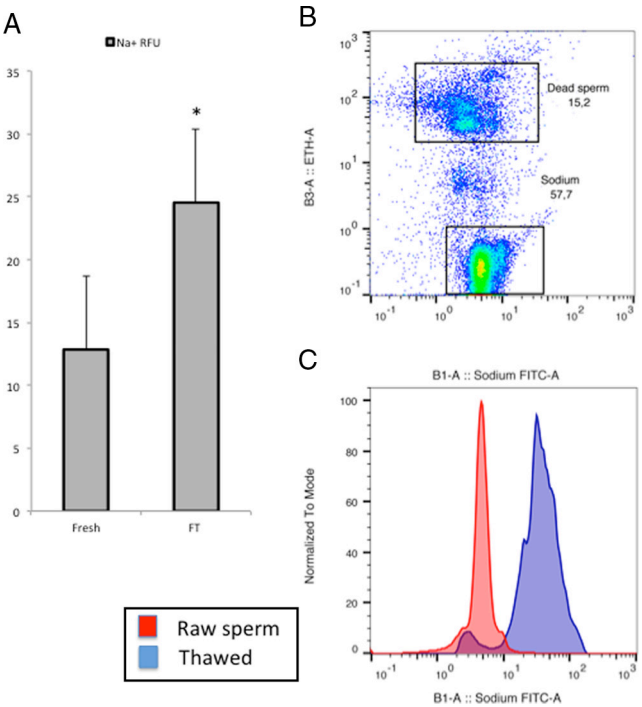

Figure 11 Changes in the content of intracellular Na+ after freezing and thawing. (A) Relative fluorescence units in raw and thawed samples $*P < 0.05$. (B) Representative cytogram of the assay, dead spermatozoa are excluded after ethidium homodimer staining, Na+ concentration is estimated with sodium green as indicated in materials and methods. (C) Overlay histograms representing intracellular Na+ in raw (red) and frozen-thawed spermatozoa (blue).

trigger in spermatozoa, oxidative stress, being opposite ends of a phenomena with a common triggering event (Aitken *et al.* 2015). Previously, we demonstrated that ROS imbalance is the key phenomena explaining apoptotic changes induced by cryopreservation (Ortega Ferrusola *et al.* 2009, Pena *et al.* 2015, Munoz *et al.* 2016). ROS imbalance leads to increased production of 4-hydroxinonenal (4-HNE) and caspase activation; however, traditional markers of oxidative stress can be reduced after cryopreservation (Martin Munoz *et al.* 2015). Our findings match with the hypothesis proposed by Aitken *et al.* (Aitken *et al.* 2015): cryopreservation leads to a transient burst of mitochondrial ROS, which initially induces capacitation in a subpopulation of spermatozoa; however, later, mitochondrial osmotic stress leads to reduced mitochondrial function with reduced ATP and stops mitochondrial ROS production. As the production of 4-HNE depends only on the initial oxidative stress and a continuous source of ω-6 fatty acids, which are very abundant in the membranes of stallion spermatozoa (Garcia *et al.* 2011, Macias Garcia *et al.* 2011), 4-HNE levels increase in spite of reduced mitochondrial ROS. Increased 4-HNE activates caspase 3 leading to sperm death in the presence of reduced ROS levels, explaining this apparent paradox.

Of special interest was the ability of the ACCENSE analysis to disclose hidden subpopulations in the ejaculate. In our study, we were able to identify subpopulations with high levels of PS externalization or groups of spermatozoa showing intense phosphorylation in tyrosine. These techniques have been used with success to identify rare subpopulations in CD8+ T cells in mouse (Shekhar *et al.* 2014) and similar techniques used to disclose intra-tumor heterogeneity in acute myeloid leukemia, linked to prognosis (Levine *et al.* 2015). Our results show that these techniques can be applied to the study of sperm biology, being able to provide relevant new information, thanks to the automatic gating and classification of spermatozoa into specific subpopulations, which are not distinguishable on biaxial plots of conventional markers.

In summary, changes induced by cryopreservation are apoptotic, with reduced mitochondrial functionality and caspase 3 activation and PS transposition as the more obvious, although a subpopulation of spermatozoa may experience capacitative changes. Moreover, we introduced for the first time computational flow cytometry tools in spermatology as being potent and promising for the study of the spermatozoa biology.

Declaration of interest

The authors declare that there is no conflict of interest that could be perceived as prejudicing the impartiality of the research reported.

Acknowledgements

The authors received financial support for this study from the Ministerio de Economía y Competitividad-FEDER, Madrid, Spain, grant AGL2013-43211-R, Junta de Extremadura-FEDER (GR 15029). PMM is supported by a pre-doctoral grant from the Ministerio de Educación, Cultura y Deporte, Madrid Spain FPU13/03991. COF is supported by a post-doctoral grant from the Ministerio de Economía y Competitividad "Juan de la Cierva" IJCI-2014-21671.

References

Aitken RJ, Baker MA & Nixon B 2015 Are sperm capacitation and apoptosis the opposite ends of a continuum driven by oxidative stress? *Asian Journal of Andrology* **17** 633–639. (doi:10.4103/1008-682X.153850)

Alvau A, Battistone MA, Gervasi MG, Navarrete FA, Xu X, Sanchez-Cardenas C, De la Vega-Beltran JL, Da Ros VG, Greer PA, Darszon A *et al*. 2016 The tyrosine kinase FER is responsible for the capacitation-associated increase in tyrosine phosphorylation in murine sperm. *Development* **143** 2325–2333. (doi:10.1242/dev.136499)

Aparicio IM, Gil MC, Garcia-Herreros M, Pena FJ & Garcia-Marin LJ 2005 Inhibition of phosphatidylinositol 3-kinase modifies boar sperm motion parameters. *Reproduction* **129** 283–289. (doi:10.1530/rep.1.00447)

Bahat A, Tur-Kaspa I, Gakamsky A, Giojalas LC, Breitbart H & Eisenbach M 2003 Thermotaxis of mammalian sperm cells: a potential navigation mechanism in the female genital tract. *Nature Medicine* **9** 149–150. (doi:10.1038/nm0203-149)

Bortner CD & Cidlowski JA 2003 Uncoupling cell shrinkage from apoptosis reveals that Na+ influx is required for volume loss during programmed cell death. *Journal of Biological Chemistry* **278** 39176–39184. (doi:10.1074/jbc.M303516200)

Buffone MG, Wertheimer EV, Visconti PE & Krapf D 2014 Central role of soluble adenylyl cyclase and cAMP in sperm physiology. *Biochimica et Biophysica Acta* **1842** 2610–2620. (doi:10.1016/j.bbadis.2014.07.013)

Caselles AB, Miro-Moran A, Morillo Rodriguez A, Gallardo Bolanos JM, Ortega-Ferrusola C, Salido GM, Pena FJ, Tapia JA & Aparicio IM 2014 Identification of apoptotic bodies in equine semen. *Reproduction in Domestic Animals* **49** 254–262. (doi:10.1111/rda.12264)

Chester C & Maecker HT 2015 Algorithmic tools for mining high-dimensional cytometry data. *Journal of Immunology* **195** 773–779. (doi:10.4049/jimmunol.1500633)

Cohen AA, Geva-Zatorsky N, Eden E, Frenkel-Morgenstern M, Issaeva I, Sigal A, Milo R, Cohen-Saidon C, Liron Y, Kam Z *et al*. 2008 Dynamic proteomics of individual cancer cells in response to a drug. *Science* **322** 1511–1516. (doi:10.1126/science.1160165)

Cormier N, Sirard MA & Bailey JL 1997 Premature capacitation of bovine spermatozoa is initiated by cryopreservation. *Journal of Andrology* **18** 461–468. (doi:10.1002/j.1939-4640.1997.tb01953.x)

Davila MP, Munoz PM, Bolanos JM, Stout TA, Gadella BM, Tapia JA, da Silva CB, Ferrusola CO & Pena FJ 2016 Mitochondrial ATP is required for the maintenance of membrane integrity in stallion spermatozoa, whereas motility requires both glycolysis and oxidative phosphorylation. *Reproduction* **152** 683–694. (doi:10.1530/REP-16-0409)

Eisenbach M 2003 Why are sperm cells phagocytosed by leukocytes in the female genital tract? *Medical Hypotheses* **60** 590–592. (doi:10.1016/S0306-9877(03)00054-9)

Eisenbach M & Giojalas LC 2006 Sperm guidance in mammals - an unpaved road to the egg. *Nature Reviews Molecular Cell Biology* **7** 276–285. (doi:10.1038/nrm1893)

Escoffier J, Krapf D, Navarrete F, Darszon A & Visconti PE 2012 Flow cytometry analysis reveals a decrease in intracellular sodium during sperm capacitation. *Journal of Cell Science* **125** 473–485. (doi:10.1242/jcs.093344)

Gallardo Bolanos JM, Miro Moran A, Balao da Silva CM, Morillo Rodriguez A, Plaza Davila M, Aparicio IM, Tapia JA, Ortega Ferrusola C & Pena FJ 2012 Autophagy and apoptosis have a role in the survival or death of stallion spermatozoa during conservation in refrigeration. *PLoS ONE* **7** e30688. (doi:10.1371/journal.pone.0030688)

Gallardo Bolanos JM, Balao da Silva CM, Martin Munoz P, Morillo Rodriguez A, Plaza Davila M, Rodriguez-Martinez H, Aparicio IM, Tapia JA, Ortega Ferrusola C & Pena FJ 2014 Phosphorylated AKT preserves stallion sperm viability and motility by inhibiting caspases 3 and 7. *Reproduction* **148** 221–235. (doi:10.1530/REP-13-0191)

Garcia BM, Fernandez LG, Ferrusola CO, Salazar-Sandoval C, Rodriguez AM, Martinez HR, Tapia JA, Morcuende D & Pena FJ 2011 Membrane lipids of the stallion spermatozoon in relation to sperm quality and susceptibility to lipid peroxidation. *Reproduction in Domestic Animals* **46** 141–148. (doi:10.1111/j.1439-0531.2010.01609.x)

Gibb Z, Lambourne SR & Aitken RJ 2014 The paradoxical relationship between stallion fertility and oxidative stress. *Biology of Reproduction* **91** 77. (doi:10.1095/biolreprod.114.118539)

Grimes ML, Lee WJ, van der Maaten L & Shannon P 2013 Wrangling phosphoproteomic data to elucidate cancer signaling pathways. *PLoS ONE* **8** e52884. (doi:10.1371/journal.pone.0052884)

Honisch S, Alkahtani S, Kounenidakis M, Liu G, Alarifi S, Al-Yahya H, Dimas K, AlKahtane AA, Prousis KC, Al-Dahmash B *et al*. 2014 A steroidal Na+/K+ ATPase inhibitor triggers pro-apoptotic signaling and induces apoptosis in prostate and lung tumor cells. *Anti-Cancer Agents in Medicinal Chemistry* **14** 1161–1168. (doi:10.2174/18715206146661406181144 18)

Iurinskaia VE, Goriachaia TS, Rubashkin AA, Shirokova AV & Vereninov AA 2010 [Changes in K+, Na+ and Cl- contents and K+ and Cl- fluxes during apoptosis of U937 cells by staurosporine. On the mechanism of cell dehydration in apoptosis]. *Tsitologiia* **52** 562–567.

Kopeika J, Thornhill A & Khalaf Y 2015 The effect of cryopreservation on the genome of gametes and embryos: principles of cryobiology and critical appraisal of the evidence. *Human Reproduction Update* **21** 209–227. (doi:10.1093/humupd/dmu063)

Levine JH, Simonds EF, Bendall SC, Davis KL, Amir el AD, Tadmor MD, Litvin O, Fienberg HG, Jager A, Zunder ER *et al*. 2015 Data-driven phenotypic dissection of AML reveals progenitor-like cells that correlate with prognosis. *Cell* **162** 184–197. (doi:10.1016/j.cell.2015.05.047)

Macias Garcia B, Gonzalez Fernandez L, Ortega Ferrusola C, Morillo Rodriguez A, Gallardo Bolanos JM, Rodriguez Martinez H, Tapia JA, Morcuende D & Pena FJ 2011 Fatty acids and plasmalogens of the phospholipids of the sperm membranes and their relation with the post-thaw quality of stallion spermatozoa. *Theriogenology* **75** 811–818. (doi:10.1016/j.theriogenology.2010.10.021)

Mair F, Hartmann FJ, Mrdjen D, Tosevski V, Krieg C & Becher B 2016 The end of gating? An introduction to automated analysis of high dimensional cytometry data. *European Journal of Immunology* **46** 34–43. (doi:10.1002/eji.201545774)

Martin Munoz P, Ortega Ferrusola C, Vizuete G, Plaza Davila M, Rodriguez Martinez H & Pena FJ 2015 Depletion of intracellular thiols and increased production of 4-hydroxynonenal that occur during cryopreservation of stallion spermatozoa lead to caspase activation, loss of motility, and cell death. *Biology of Reproduction* **93** 143. (doi:10.1095/biolreprod.115.132878)

Munoz PM, Ferrusola CO, Lopez LA, Del Petre C, Garcia MA, de Paz Cabello P, Anel L & Pena FJ 2016 Caspase 3 activity and lipoperoxidative status in raw semen predict the outcome of cryopreservation of stallion spermatozoa. *Biology of Reproduction* **95** 53. (doi:10.1095/biolreprod.116.139444)

Newman JR & Weissman JS 2006 Systems biology: many things from one. *Nature* **444** 561–562. (doi:10.1038/nature05407)

Newman JR, Ghaemmaghami S, Ihmels J, Breslow DK, Noble M, DeRisi JL & Weissman JS 2006 Single-cell proteomic analysis of S. cerevisiae reveals the architecture of biological noise. *Nature* **441** 840–846. (doi:10.1038/nature04785)

Newton H 1998 The cryopreservation of ovarian tissue as a strategy for preserving the fertility of cancer patients. *Human Reproduction Update* **4** 237–247. (doi:10.1093/humupd/4.3.237)

Nunez-Martinez I, Moran JM & Pena FJ 2006 A three-step statistical procedure to identify sperm kinematic subpopulations in canine ejaculates: changes after cryopreservation. *Reproduction in Domestic Animals* **41** 408–415. (doi:10.1111/j.1439-0531.2006.00685.x)

Nunez-Martinez I, Moran JM & Pena FJ 2007 Identification of sperm morphometric subpopulations in the canine ejaculate: do they reflect different subpopulations in sperm chromatin integrity? *Zygote* **15** 257–266. (doi:10.1017/S0967199407004248)

Orlov SN, Platonova AA, Hamet P & Grygorczyk R 2013 Cell volume and monovalent ion transporters: their role in cell death machinery triggering and progression. *American Journal of Physiology: Cell Physiology* **305** C361–C372. (doi:10.1152/ajpcell.00040.2013)

Ortega-Ferrusola C, Sotillo-Galan Y, Varela-Fernandez E, Gallardo-Bolanos JM, Muriel A, Gonzalez-Fernandez L, Tapia JA & Pena FJ 2008 Detection of "apoptosis-like" changes during the cryopreservation process in equine sperm. *Journal of Andrology* **29** 213–221. (doi:10.2164/jandrol.107.003640)

Ortega Ferrusola C, Gonzalez Fernandez L, Morrell JM, Salazar Sandoval C, Macias Garcia B, Rodriguez-Martinez H, Tapia JA & Pena FJ 2009 Lipid peroxidation, assessed with BODIPY-C11, increases after cryopreservation of stallion spermatozoa, is stallion-dependent and is related to apoptotic-like changes. *Reproduction* **138** 55–63. (doi:10.1530/REP-08-0484)

Ortega-Ferrusola C, Macias Garcia B, Suarez Rama V, Gallardo-Bolanos JM, Gonzalez-Fernandez L, Tapia JA, Rodriguez-Martinez H & Pena FJ 2009 Identification of sperm subpopulations in stallion ejaculates: changes after cryopreservation and comparison with traditional statistics. *Reproduction in Domestic Animals* **44** 419–423. (doi:10.1111/j.1439-0531.2008.01097.x)

Ortega Ferrusola C, Gonzalez Fernandez L, Salazar Sandoval C, Macias Garcia B, Rodriguez Martinez H, Tapia JA & Pena FJ 2010 Inhibition of the mitochondrial permeability transition pore reduces "apoptosis like" changes during cryopreservation of stallion spermatozoa. *Theriogenology* **74** 458–465. (doi:10.1016/j.theriogenology.2010.02.029)

Pena FJ, Johannisson A, Wallgren M & Rodriguez-Martinez H 2003 Assessment of fresh and frozen-thawed boar semen using an e assay: a new method of evaluating sperm membrane integrity. *Theriogenology* **60** 677–689. (doi:10.1016/S0093-691X(03)00081-5)

Pena FJ, Saravia F, Nunez-Martinez I, Johannisson A, Wallgren M & Rodriguez Martinez H 2006 Do different portions of the boar ejaculate vary in their ability to sustain cryopreservation? *Animal Reproduction Science* **93** 101–113. (doi:10.1016/j.anireprosci.2005.06.028)

Pena FJ, Rodriguez Martinez H, Tapia JA, Ortega Ferrusola C, Gonzalez Fernandez L & Macias Garcia B 2009 Mitochondria in mammalian sperm physiology and pathology: a review. *Reproduction in Domestic Animals* **44** 345–349. (doi:10.1111/j.1439-0531.2008.01211.x)

Pena FJ, Garcia BM, Samper JC, Aparicio IM, Tapia JA & Ferrusola CO 2011 Dissecting the molecular damage to stallion spermatozoa: the way to improve current cryopreservation protocols? *Theriogenology* **76** 1177–1186. (doi:10.1016/j.theriogenology.2011.06.023)

Pena FJ, Plaza Davila M, Ball BA, Squires EL, Martin Munoz P, Ortega Ferrusola C & Balao da Silva C 2015 The impact of reproductive technologies on stallion mitochondrial function. *Reproduction in Domestic Animals* **50** 529–537. (doi:10.1111/rda.12551)

Pena FJ, Muñoz PM & Ortega-Ferrusola C 2016*a* Flow cytometry probes to evaluate stallion spermatozoa. *Journal of Equine Veterinary Science* **43** S23–S28. (doi:10.1016/j.jevs.2016.06.004)

Pena FJ, Ortega Ferrusola C & Martin Munoz P 2016*b* New flow cytometry approaches in equine andrology. *Theriogenology* **86** 366–372. (doi:10.1016/j.theriogenology.2016.04.050)

Plaza Davila M, Martin Munoz P, Tapia JA, Ortega Ferrusola C, Balao da Silva CC & Pena FJ 2015 Inhibition of mitochondrial complex I leads to decreased motility and membrane integrity related to increased hydrogen peroxide and reduced ATP production, while the inhibition of glycolysis has less impact on sperm motility. *PLoS ONE* **10** e0138777. (doi:10.1371/journal.pone.0138777)

Pons-Rejraji H, Bailey JL & Leclerc P 2009 Cryopreservation affects bovine sperm intracellular parameters associated with capacitation and acrosome exocytosis. *Reproduction, Fertility, and Development* **21** 525–537. (doi:10.1071/RD07170)

Saadatpour A, Lai S, Guo G & Yuan GC 2015 Single-cell analysis in cancer genomics. *Trends in Genetics* **31** 576–586. (doi:10.1016/j.tig.2015.07.003)

Salicioni AM, Platt MD, Wertheimer EV, Arcelay E, Allaire A, Sosnik J & Visconti PE 2007 Signalling pathways involved in sperm capacitation. *Society for Reproduction and Fertility* **65** 245–259.

Sapia L, Palomeque J, Mattiazzi A & Petroff MV 2010 Na+/K+-ATPase inhibition by ouabain induces CaMKII-dependent apoptosis in adult rat cardiac myocytes. *Journal of Molecular and Cellular Cardiology* **49** 459–468. (doi:10.1016/j.yjmcc.2010.04.013)

Shekhar K, Brodin P, Davis MM & Chakraborty AK 2014 Automatic Classification of Cellular Expression by Nonlinear Stochastic Embedding (ACCENSE). *PNAS* **111** 202–207. (doi:10.1073/pnas.1321405111)

Sigal A, Milo R, Cohen A, Geva-Zatorsky N, Klein Y, Liron Y, Rosenfeld N, Danon T, Perzov N & Alon U 2006 Variability and memory of protein levels in human cells. *Nature* **444** 643–646. (doi:10.1038/nature05316)

Spiegel I, Adamsky K, Eisenbach M, Eshed Y, Spiegel A, Mirsky R, Scherer SS & Peles E 2006 Identification of novel cell-adhesion molecules in peripheral nerves using a signal-sequence trap. *Neuron Glia Biology* **2** 27–38. (doi:10.1017/S1740925X0600007X)

Yeste M, Estrada E, Rocha LG, Marin H, Rodriguez-Gil JE & Miro J 2015 Cryotolerance of stallion spermatozoa is related to ROS production and mitochondrial membrane potential rather than to the integrity of sperm nucleus. *Andrology* **3** 395–407. (doi:10.1111/andr.291)

Received 3 October 2016
First decision 24 October 2016
Revised manuscript received 2 November 2016
Accepted 12 December 2016